International Journal of Applied and Natural Sciences (IJANS)
ISSN (P): 2319-4014; ISSN (E): 2319-4022
Vol. 3, Issue 3, May 2014, 15-36

International Academy of Science, Engineering and Technology
Connecting Researchers; Nurturing Innovations

STUDY OF BEHAVIOUR AND NATURE OF DOPING HOLES IN UNDER DOPED AND OVERDOPED REGIMES CUPRATE PEROVSKITES

SUMIT KUMAR GUPTA

Department of Physics, Maharishi Arvind Institute of Engineering & Technology, Jaipur, Rajasthan, India

ABSTRACT

After more than 15 years of intense research since the discovery of high-temperature superconductivity [1], many interesting physical phenomena unique to the cuprate superconductors are better understood, and various applications have been realized. However, the underlying mechanism for high-temperature superconductivity remains elusive, largely due to the complication of numerous competing orders in the ground state of the cuprates. We review some of the most important physics issues and recent experimental developments associated with these strongly correlated electronic systems, and discuss current understanding and possible future research direction.

KEYWORDS: Cuprate Superconductors, High, Temperature Superconductivity

1. INTRODUCTION

High-temperature superconducting cuprates are doped Mott insulators with numerous competing orders in the ground state [2-5]. Mott insulators differ from conventional band insulators in that the latter are dictated by the Pauli exclusion principle when the highest occupied band contains two electrons per unit cell, whereas the former are associated with the existence of strong on-site Coulomb repulsion such that double occupancy of electrons per unit cell is energetically unfavourable and the electronic system behaves like an insulator rather than a good conductor at half filling. An important signature of doped Mott insulators is the strong electronic correlation among the carriers and the sensitivity of their ground state to the doping level.

In cuprates, the ground state of the undoped perovskite oxide is an antiferromagnetic Mott insulator, with nearest-neighbour Cu^{2+}-Cu^{2+} antiferromagnetic exchange interaction in the CuO_2 planes [6]. Depending on doping with either electrons or holes into the CuO_2 planes [6, 7], the Neel temperature (T_N) for the antiferromagnetic to-paramagnetic transition decreases with increasing doping level. Upon further doping of carriers, long-range ant ferromagnetism vanishes and is replaced by superconductivity. As shown in the phase diagrams for the hole-doped (p-type)and electron-doped (n-type) cuprates in Figure 1, the

Superconducting transition temperature (T_c) first increases with increasing doping level (δ), reaching a maximum T_c at an optimal doping level, then decreases and finally vanishes with further increase of doping. Although the phase diagrams appear similar for both p-type and n-type cuprates, they are in fact not truly symmetric. For *p*-type cuprates in the under- and optimally doped regime, the normal state properties below a crossover temperature T^* are significantly different from those of Fermi liquid, and the electronic density of states (DOS) appear to be slightly suppressed [8]. These unconventional normal state properties are referred to as the pseudogap phenomenon [8]. Moreover, holes enter into

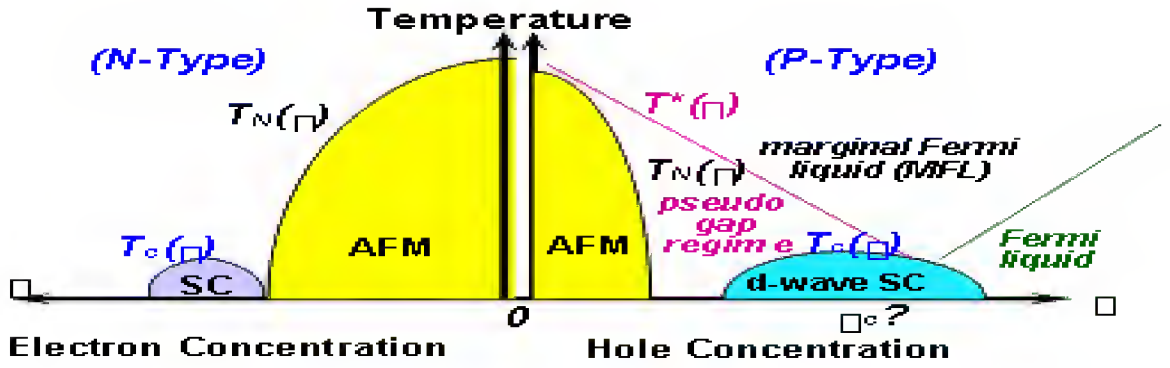

Figure 1: Generic Temperature (T) vs. Doping Level (δ) Phase Diagrams of p-Type and n-Type Cuprates in Zero Magnetic Field (AFM: Antiferromagnetic Phase; SC: Superconducting Phase; T_N, T_c and T* Are the Neel, Superconducting and Pseudo Gap Transition Temperatures, Respectively)

the oxygen *p*-orbital in the CuO_2 planes, which induce ferromagnetic coupling for the Cu^{2+} ions adjacent to the partially empty oxygen orbital, thus resulting in significant spin frustrations in the CuO_2 planes, as schematically illustrated in Figure 2(a) for a specific 1/8-doping level. The resulting strong spin fluctuations are the primary cause for the rapid decline of the Neel state with increasing hole doping. On the other hand, electron doping in n-type cuprates takes place in the *d*-orbital of Cu, giving rise to spinless Cu^{+}-ions that dilute the

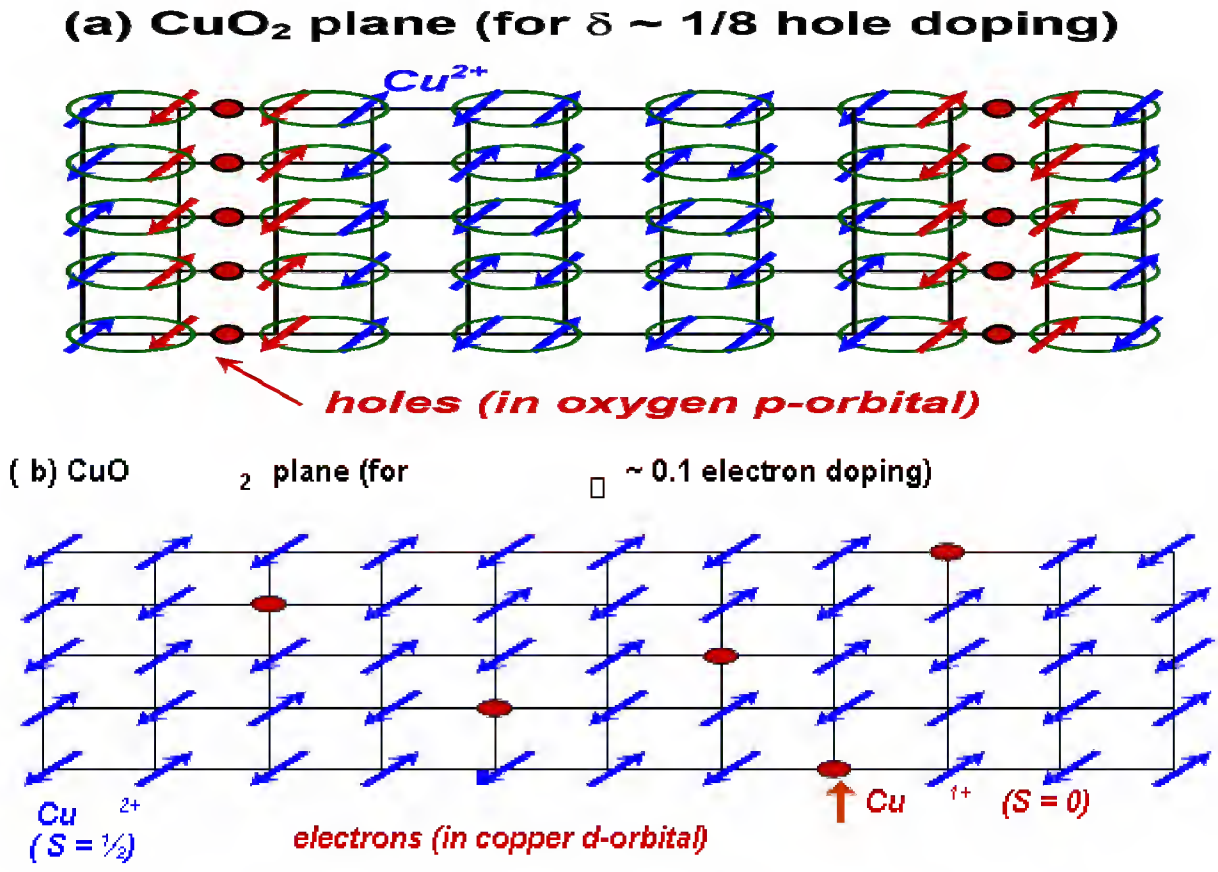

Figure 2: Effects of Hole and Electron Doping on the Spin Configurations in the CuO_2 Plane. (a) Doped Holes are Associated with the Oxygen p-Orbital, which Result in Ferromagnetic 2+Coupling Ions, Yielding Strong Spin between the Neighbouring Cu Frustrations in the CuO_2 Plane. For a Special 1/8 Doping Level, Charge Stripes can be Formed as Illustrated (b) Doped Electrons Are Associated of Cu, Yielding Cu + with the d-Orbital that Dilutes the Antiferro Magnetic of the Undoped Sample without Causing Significant Spin Frustrations

background antiferromagnetic Cu^{2+}-Cu^{2+} coupling without inducing as strong spin frustrations as those in the p-type cuprates, as shown in Figure 2(b). Hence, the Neel state survives over a larger range of electron doping, in contrast to the p-type cuprates, whereas the superconducting phase in the n-type cuprates exists over a much narrower doping range relative to the p-type cuprates. Other important contrasts between the n-type and p-type cuprates include the absence of pseudo gap phenomena in the former [9-12], non-universal pairing symmetries [9-22], and different doping dependent Fermi surface evolution according to the angular-resolved photoemission spectroscopy (ARPES) [23]. The lack of electron-hole symmetry suggests that the cuprates cannot be fully described by a one-band Hubbard or *t-J* model.

Concerning the competing orders in the ground state of the cuprates, besides the obvious SU(2) and U(1) broken symmetries associated with the occurrence of antiferromagnetism and superconductivity, respectively, other competing orders include the crystalline symmetry ($\mathcal{C}$) and the time-reversal ($\mathcal{T}$) symmetry [3,4]. These competing orders in the two-dimensional one-band square-lattice approximation can give rise to a large variety of doping-dependent ground states [3,4]. For instance, charge stripes can exist under specific doping levels (e.g. 1/8), as exemplified in

Figure 2(a), which have observed in some underdoped cuprates [24-28]. Another possible ground state is the *d*-density wave (DDW) state also known as orbital antiferromagnetism [29], which involves alternating orbital currents from one plaque to the adjacent plaque [29,30]. The DDW state is a broken $\mathcal{T}$ -symmetry state, which in principle can be verified experimentally [29], although to date no conclusive empirical evidence has been found. Other possible ground states based on the simplified mean-field and two-dimensional square-lattice approximations include the spinPierrl state, Wigner crystal state, spin density waves (SDW), charge density waves (CDW), and complex pairing symmetry of (d_x2-$_y2$+id_{xy}) or (d_x2y2+is), depending on the doping level and the Coulomb and exchange interaction strengths [3,4]. The large varieties of ground states are indicative of the complex nature of competing orders in the cuprates. It is therefore imperative to identify universal characteristics among all cuprates and to develop understanding for the differences in order to unravel the underlying pairing mechanism for cuprate superconductivity.

2. NEW EXPERIMENTAL DEVELOPMENT

In this section we review some of the recent experimental developments that provide important new information for the microscopic descriptions of cuprate superconductivity. Special emphasis will be placed on the issues of competing orders, non-universal pairing symmetry, different lowenergy excitations and response to quantum impurities among the p-type and n-type cuprates, and possible physical origin of the pseudogap phenomenon.

2.1. Quantum Impurities in P-Type Cuprate Superconductors

Magnetic quantum impurities are known to suppress conventional superconductivity, and the detailed effects have been a topic of great research interest over the years [75-79]. In contrast, nonmagnetic impurities in the dilute limit are found to have negligible effects on conventional superconductivity [80]. However, recent findings of strong effects of spinless quantum impurities on p-type cuprate superconductors [15, 81-92] have rekindled active investigation on the effects of quantum impurities on superconductivity.

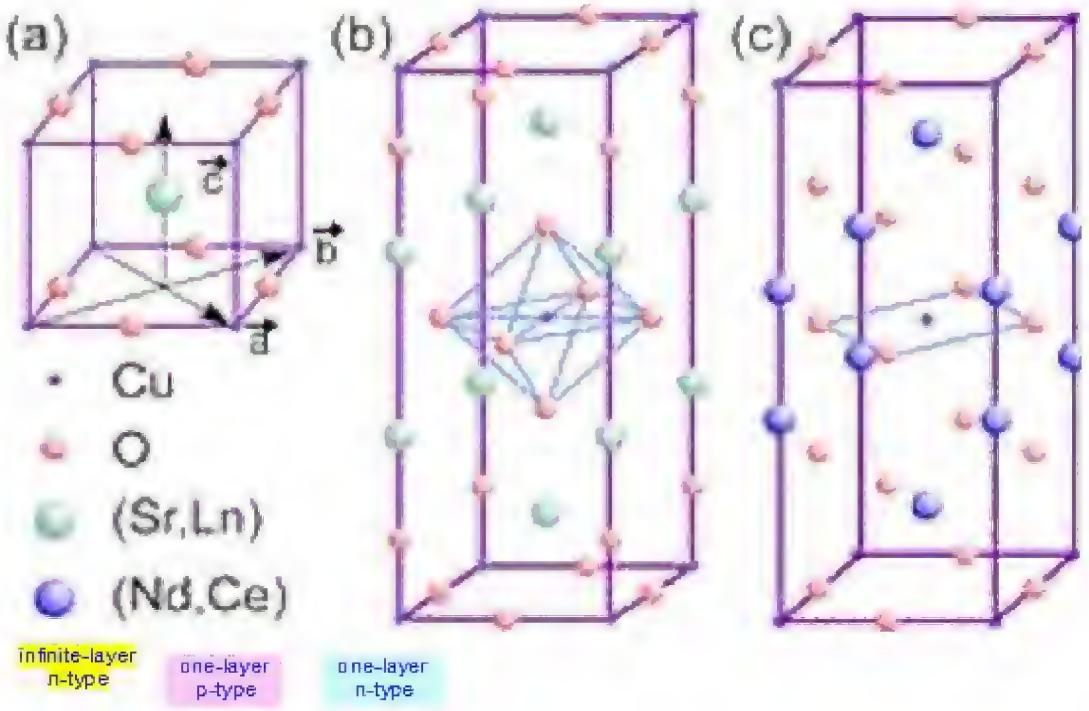

Figure 3: Comparison of the Crystalline Structures of Representative p-Type and n-Type Cuprates. We Note the Absence of Apical Oxygen in All n-Type Cuprates, in Contrast to the Existence of CuO_6 Octahedron or its Variations in All Type Cuprates. Moreover, the Infinite-Layer System Differs from all Other Cuprates in that there is No Excess Block of Charge Reservoir between Consecutive CuO_2 Planes

Generally speaking, the effects of quantum impurities on superconductivity depend on the pairing symmetry and the existence of magnetic correlation in cuprate superconductors [93-101]. For instance, Fermionic nodal quasiparticles in the cuprates with either $d_{x^2-y^2}$ or $(d_{x^2-y^2}+s)$ pairing symmetry can interact strongly with the quantum impurities in the CuO_2 planes and incur significant suppression of superconductivity regardless of the spin configuration of the impurity [93-97], in stark contrast to the insensitivity to spinless impurities in conventional *s*-wave superconductors [80]. Moreover, the spatial evolution of the quasiparticle spectra near quantum impurities would differ significantly if a small component of complex order parameter existed in the cuprate [98]. For instance, should the pairing symmetry contain a complex component such as $(d_{x^2-y^2}+id_{xy})$ that broke the $\mathcal{T}$-symmetry, the quasiparticle spectrum at a spinless impurity site would reveal two resonant scattering peaks at energies of equal magnitude but opposite signs in the electron-like and hole-like quasiparticle branches [98]. In contrast, for either $d_{x^2-y^2}$ or $(d_{x^2-y^2}+s)$ pairing symmetry [15, 92], only one resonant scattering peak at the impurity site is expected for large potential scattering strength [93-97]. In addition, the existence of nearest-neighbour Cu^{2+}-Cu^{2+} antiferromagnetic coupling in the superconducting state of the cuprates can result in an unusual Kondo-like behaviour near a spinless impurity [82,84,88-91,100,101] due to induced spin-1/2 moments on the neighbouring Cu^{2+}-ions that surround the Cu-site substituted with a spinless ion such as Zn^{2+}, Mg^{2+}, Al^{3+} and Li^{+} [82,84, 88-91], as schematically illustrated in Figure 4.

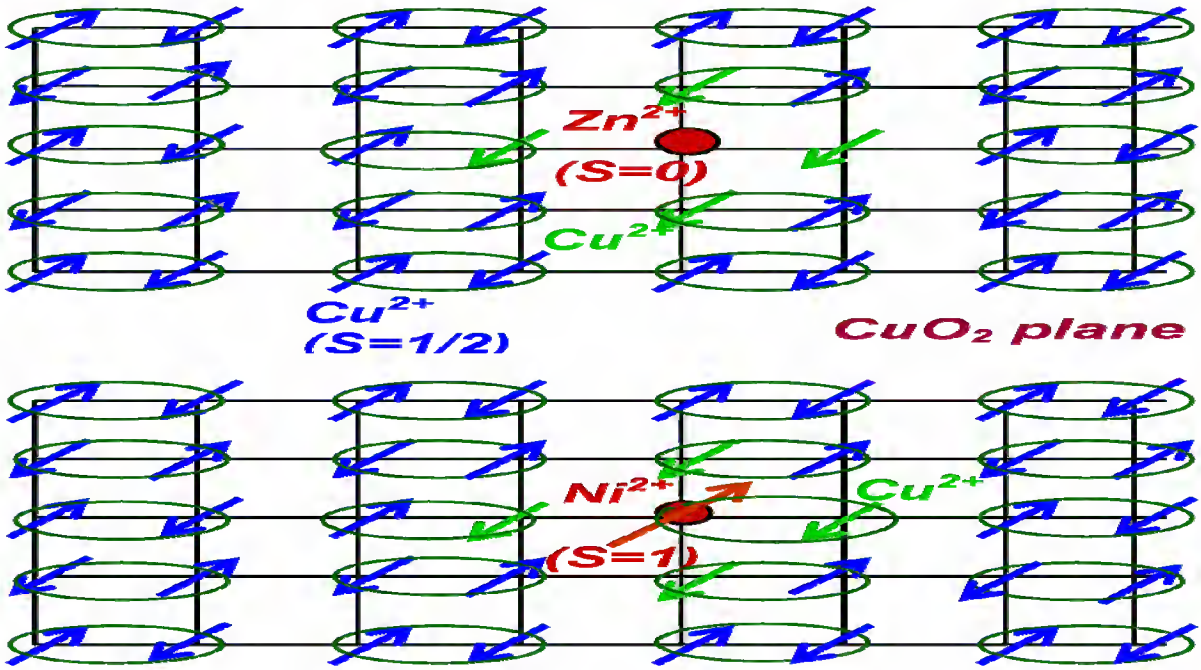

Figure 4: Effects of Quantum Impurities on p-Type Cuprate Superconductors in the Underdoped Limit. Upper Panel: Induced Magnetic Moments on the Neighbouring Cu^{2+}Sites Surrounding a Spinless Impurity (Such as Zn^{2+}, Mg^{2+}, Al^{3+}, and Li^{+} with S = 0) in p-Type Cuprates. Lower Panel: A Localized Ni^{2+} Impurity Coexisting with the Background AFM Coupling in the CuO_2 Plane

Empirically, the Kondo-like behaviour associated with isolated spinless impurities in p-type cuprates has been confirmed from the nuclear magnetic resonance (NMR) and inelastic neutron scattering experiments, and the spinless impurities are found to have more significant effects on broadening the NMR line width, damping the collective magnetic excitations and reducing the superfluid density than magnetic impurities such as Ni^{2+} with $S = 1$ [82, 84, 88-91]. On the other hand, both types of impurities exhibit similar global effects on suppressing T_c, increasing the microwave surface resistance in the superconducting state and increasing the normal state resistivity [81-102]. The stronger suppression of superconductivity due to spinless impurities in *d*-wave cuprates can be attributed to the slower spatial relaxation of spin polarization near the spinless impurities than that near the $S = 1$ impurities due to the delocalized spatial distribution of the induced moments in the former [99-101], as illustrated in Figure 4.

Detailed spatial evolution of the quasiparticle tunnelling spectra near these quantum impurities in the cuprates can provide useful information for the pairing state of the cuprates, and has recently been investigated in impurity-substituted $Bi_2Sr_2CaCu_2O_{8+}\delta$ (Bi-2212) [92,102] and $YBa_2Cu_3O_{7-}\delta$ (YBCO) [10] systems using lowtemperature scanning tunnelling microscopy (STM). While in principle both the potential scattering and the Kondo effect contribute to the quasiparticle spectra near spinless impurities, which of the two contributions may be dominant depends on the doping level [101] and cannot be easily determined because direct probing of the quasiparticle spectra near the quantum impurities with scanning tunnelling spectroscopy (STS) involves not only the density of states in the CuO_2 planes of the cuprates but also the tunnelling matrix [100,101]. The tunnelling matrix depends on the atomic structure of the surface layers and the exact path of the tunnelling quasiparticles [100], which is difficult to determine empirically.

Nonetheless, one can still derive useful information from the STM experimental data by the following simplified consideration. If one 1) neglects many-body interactions in the cuprates, 2) limits the effect of quantum impurities to perturbative and one-band approximation without solving for the spatially varying pairing potential self-consistently [101],

and 3) disregards the interaction among impurities, one can describe the effect of quantum impurities with the Hamiltonian $\mathcal{H} = \mathcal{H}_{BCS} + \mathcal{H}_{imp}$. Here H_{BCS} denotes the $d_{x^2-y^2}$wave BCS Hamiltonian [101] that contains the normal (diagonal) one-band single-particle Eigen energy and anomalous (off-diagonal) $d_{x^2-y^2}$-wave pairing potential Δ_k (= $\Delta_d \cos 2\theta_k$, θ_k being the angle relative to the anti-node of the order parameter in the momentum space)of the unperturbed host, and $\mathcal{H}_{imp} = \mathcal{H}_{pot} + \mathcal{H}_{mag}$ denotes the impurity perturbation due to both the localized potential scattering term H_{pot} (= $U\sum_\sigma c\sigma\ c\sigma$; U: the on-site Coulomb scattering potential) and the Kondo-like magnetic exchange interaction term $\mathcal{H}_{mag}$ (= $\sum_{\mathbf{R}} J\ \mathbf{RS}\bullet\sigma_{\mathbf{R}}$) between the spins of the conduction carriers on the **R** sites ($\sigma_{\mathbf{R}}$) and those of the localized magnetic moments (S).

The above Hamiltonian can be used to obtain the quasiparticle spectra associated with quantum impurities in$d$-wave superconductors by means of Green's function techniques. If one further neglects contributions from the tunnelling matrix, one obtains a single resonant energy at Ω_0 on the impurity site in either pure potential scattering limit for a point impurity or pure magnetic scattering limit for four induced moments associated with one spinless impurity [93-97]. For pure potential scattering, one has [94,95]:

$$|\Omega_0/\Delta_d| \approx [(\pi/2\cot\delta_0 / \ln(8/\pi\cot\delta_0)], \quad (1)$$

Whereδ_0 is the impurity-induced phase shift in the quasiparticle wave function of a $d_{x^2-y^2}$-wave superconductor, and $\delta_0 \rightarrow (\pi/2)$ in the strong potential scattering (unitary) limit. Moreover, the intensity of the resonant scattering is expected to decay rapidly within approximately one Fermi wavelength, and the spatial evolution of the quasiparticles spectra under a given bias voltage V = (Ω_0/e) should reveal 4-fold symmetry of the underlying lattice. Indeed, the spatially resolved STS studies of spinless impurities in optimally doped YBCO and Bi-2212 systems are in reasonable agreement with theoretical predictions for $d_{x^2-y^2}$-wave superconductors [15,92], although whether potential scattering or Kondo effect may be more important has not been determined conclusively. Representative tunnelling spectra associated with either Zn^{2+} or Mg^{2+} impurities in YBCO are illustrated in Figure 8. On the other hand, for magnetic impurities with both contributions from $\mathbf{H}_{pot}$ and $\mathbf{H}_{mag}$, there are two spin-polarized impurity states at energies $\pm\Omega_{1,2}$ [96]:

$$|\Omega_{1,2}/\Delta_d| = 1/[2N_F(U\pm W\ln|8\ N_F(U\pm W)|], \quad (2)$$

WhereN_F denotes the density of states at the Fermi level and $W \equiv JS\bullet\sigma$ implies that magnetic impurities are isolated and equivalent at all sites. This prediction for magnetic impurities in $d_{x^2-y^2}$wave superconductors has been verified by STS studies of Ni-substituted Bi-2212 single crystals [102], and the results are in stark contrast to those of magnetic impurities in conventional s-wave superconductors [103,104]. In the latter case, the irrelevance of potential scattering yields only one magnetic impurity-induced bound-state energy at $\pm|\Omega_B|$ and $|\Omega_B|<\Delta_0$, where$\Delta_0$is the s-wave pairing potential, and $|\Omega_B|$ is given by [76]:

$$|\Omega_B/\Delta_0| = (\pi/2)\ JSN_F. \quad (3)$$

Despite overall similarities in their response to quantum impurities, detailed STS studies of the Bi-2212 and YBCO systems still revealed some interesting differences [15, 92]. First, the global superconducting gap Δ_d was suppressed to (25 ± 2) meV due to non-magnetic impurities from Δ_d= (29 ± 1) meV in pure YBCO [15], whereas the global effect of Zn on Bi-2212 could not be determined because of the strong spatial variations in the tunnelling gap values of Bi-2212 [105,106]. Second, the energy ω_{dip} associated with the "dip hump" satellite features (see Figure 5(a)) also shifted substantially relative to that in pure YBCO, whereas such an effect could not be quantified in Bi-2212. The dip-hump

feature has been attributed to quasiparticle damping by the background many body excitations such as incommensurate spin fluctuations [107,108], triplet particle-particle excitations [5,52] or phonons [109], and the resonant energy of the many-body excitation may be empirically given by $|\Omega_{res}| = |\omega_{dip}\delta - \Delta_d|$. We find that the magnitude of Ω_{res} in the (Zn, Mg)-YBCO sample decreased significantly to (7 ± 1) meV from that in the pure YBCO where $|\Omega_{res}| = (17 \pm 1)$ meV.

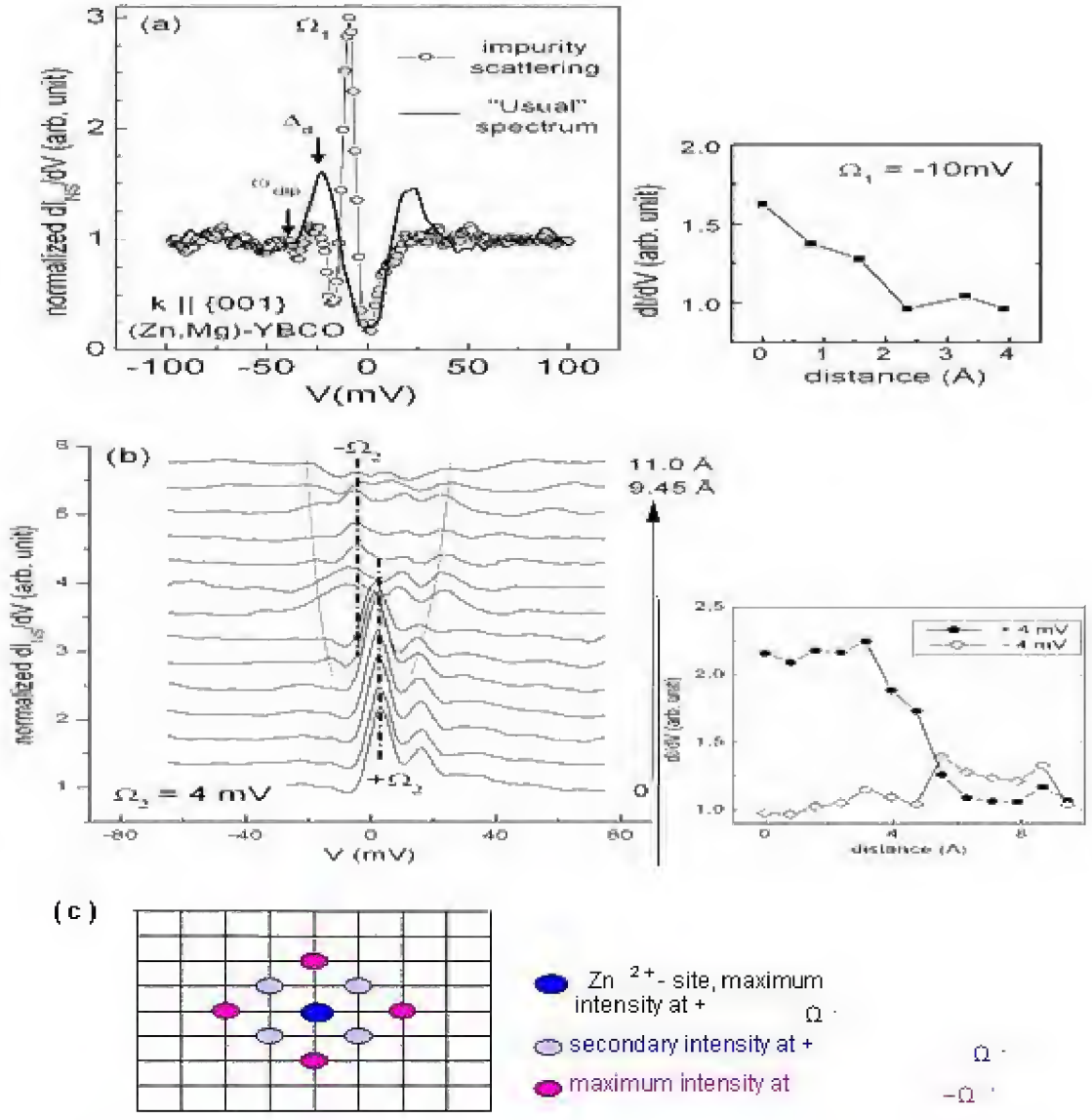

Figure 5: Normalized c-Axis Quasiparticle Spectra of an Optimally Doped YBCO near Zn^{2+} or Mg^{2+}Impurity at 4.2 K. (a) Left Panel: An Impurity Scattering Spectrum with a Resonant Peak at $\Omega_1 \sim -10$ meV and a Typical C-Axis Spectrum Far Away from Impurities. Right Panel: Spatial Variation of the Impurity-Induced Resonant Peak Intensity (b) Left Panel: Representative Spectra Revealing Spatial Variations in the Quasiparticle Spectra along the Cu-O Bonding Direction from an Impurity with a Maximum Scattering at $\Omega_2 \sim +4$ me V. We Note the Alternating Resonant Peak Energies between + 4 meV and – 4 meV and the Particle-Hole Asymmetry in the Degrees of Suppression of the Superconducting Coherence Peaks. Right Panel: Spatial Variation of the Impurity Induced Resonant Peak Intensity at $-\Omega_2$ (c) Theoretical Predictions [101] for the Spatial Variations of the Impurity Scattering Intensity at Resonant Energies $-\Omega$ on the CuO_2 Plane

This drastic decrease in Ω_{res} with the very small impurity concentration (<1%) in our Zn and Mg-substituted YBCO has clearly ruled out phonons as the relevant many-body excitations to the satellite features [9, 15]. On the other hand, the induced moments due to spinless impurities can suppress the gapped spin fluctuations in the CuO_2 planes by

randomizing the AFM spin correlation. Third, details of the local spectral evolution near the impurity site also vary somewhat between the Bi-2212 and YBCO systems [15, 92]. For instance, the range of impurity effect is longer (~ 3 nm) in YBCO [15] relative to that in Bi-2212 (~ 1.5 nm) [92]. Moreover, the resonant scattering peak in YBCO appears to alternate between energies of the same magnitude and opposite signs near some of the impurities [113], as exemplified in the left panel of Figure 5(b). Such spatial variations are expected for both Kondo-like and charge-like impurities in *d*-wave superconductors [101].

The response of p-type cuprates such as YBCO [15] and Bi-2212 systems [92] to quantum impurities is empirically in agreement with a pairing state that is gapless along the (–π,–π) momentum directions, regardless of the relative strength of potential scattering and magnetic exchange interaction. Therefore the tunnelling spectroscopic studies of pure and impurity substituted p-type cuprates all suggest that the pairing symmetry of p-type cuprates is consistent with pure $d_{x^2-y^2}$ for tetragonal crystals or ($d_{x^2-y^2}+s$) for orthorhombic crystals [15, 16, 69, 92,102,113], both symmetries involving nodes in the pairing potential along (–π,–π). These studies place an upper bound of less than 5% for any secondary complex pairing component [15, 16, 69].

2.2. Strongly Correlated S-Wave Pairing in the Infinite-Layer N-Type Cuprates

As discussed earlier in Section 2.2, the pairing symmetry in the n-type cuprates appears to be non-universal and doping dependent [9, 10, 17-20]. In particular, the simplest form of cuprate superconductors [114,115], known as the infinite-

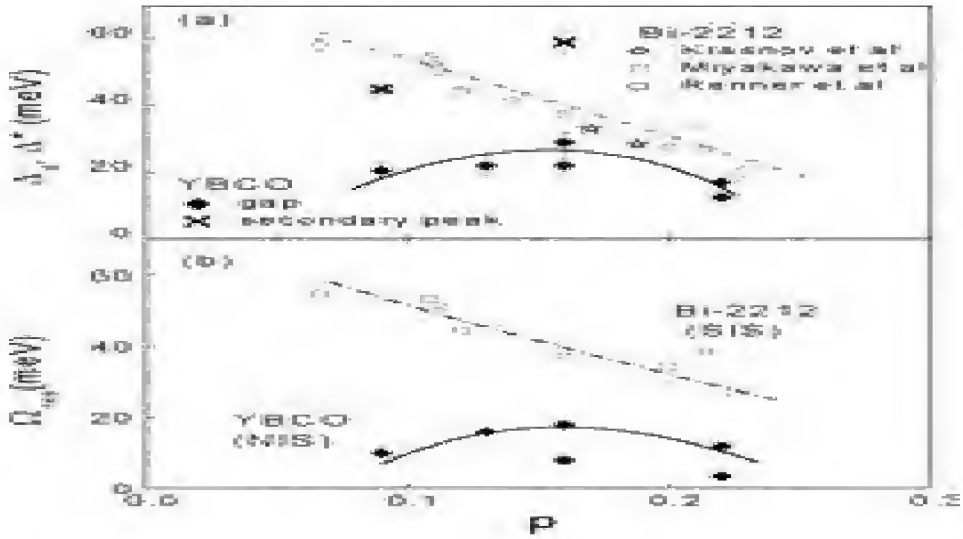

Figure 6: (a) The Tunnelling Gap $\Delta_d(p)$ of YBCO, as Determined from STS Measurements, is Compared with the Measured Gap$\Delta^*(p)$ in Bi-2212 from Various Techniques, Including Direct Measurements on Mesa Structures (Krasnov et al. [110]), Point Contact and S-IS Break-Junction Measurements (Miyakawa et al. [111]) and STS Studies (Renner et al. [112]). The Doping Level p, Except for the Optimally Doped (Zn, Mg)-YBCO, is Estimated by Means of an Empirical Formula $T_c = T_{c,max}[1-82.6\ (p-0.16)^2]$, with $T_{c,max} = 93.0$ K for the Optimally Doped YBCO. The Global Value of Δ_d in the Optimally Doped (Zn, Mg)-YBCO is Reduced Relative to that of Pure YBCO (b) Comparison of Ω_{res} (p) and Ω_2 (p) for YBCO and Bi-2212. Note the Resemblance of Ω_{res} (p) to Δ_d (p) and the Significant Suppression of Ω_{res} due to Spinless Impurities

Layer n-type cuprates $Sr_{1-x}Ln_xCuO_2$ (where Ln = La, Gd, Sm, see Figure 3), reveal strong spectroscopic evidences for a pure *s*-wave pairing symmetry, although the pairing state still differ significantly from conventional weak-coupling characteristics [9, 10,113]. In this subsection, we summarize the experimental evidence for strongly correlated *s*-wave

superconductivity in the infinite-layer system. The specific aspects for consideration include: 1) momentum-independent quasiparticle tunnelling spectra and the absence of satellite features, 2) conventional response to quantum impurities, and 3) consistency of magnetic impurity-induced bound states with the Shiba states for *s*-wave superconductors. We also critically examine the relevance of pseudogap to cuprate superconductivity, particularly given the absence of pseudogap in all n-type cuprates under zero magnetic field [9-12].

Concerning the issue of pairing symmetry, it is feasible that the pairing symmetry of p-type cuprates favour $d_{x^2-y^2}$-wave over *s*-wave in order to minimize the on-site Coulomb repulsion and the orbital potential energy while maintaining the quasi-two dimensionality, because the presence of apical oxygen in p-type cuprates (see Figure 3) lifts the degeneracy of $d_{x^2-y^2}$ and $d_{3z^2-r^2}$ orbitals in favour of $d_{x^2-y^2}$-orbital for holes, as discussed earlier. On the other hand, the absence of apical oxygen in the n-type cuprates retains the degeneracy of $d_{x^2-y^2}$ and $d_{3z^2-r^2}$, thus favouring a more three-dimensional pairing. In the case of one-layer n-type cuprates, the large separation between consecutive CuO_2 planes could still favour a $d_{x^2-y^2}$-wave pairing symmetry that preserves the quasi-two dimensionality, although the exact pairing symmetry in a specific cuprate depends on the subtle balance of competing energy scales as a function of electron doping and also on the degree of oxygen disorder in the interstitial sites between CuO_2 planes.

In contrast, the infinite-layer n-type cuprates such as $Sr_{0.9}La_{0.1}CuO_2$ differ from other cuprates in a number of ways. First, the infinite-layer system contains only one metallic monolayer of Sr or La rather than a large charge reservoir as in other cuprates between consecutive CuO_2 planes. Second, the c-axis superconducting coherence length (ξ_c ~ 0.53 nm) is longer than the c-axis lattice constant (c_0) [116,117], in contrast to the typical condition of $\xi_c << c_0$ in most other cuprates. Hence, the infinite-layer system is expected to reveal more three-dimensional characteristics. Third, Knight-shift experiments [11] have revealed that the carrier density of the optimally doped $Sr_{0.9}La_{0.1}CuO_2$ at the Fermi level is significantly smaller than that in typical p-type cuprates, being ~ 25% that of optimally doped $YBa_2Cu_3O_{7-\delta}$. These atypical characteristics of the infinite-layer system are suggestive of a tendency towards more isotropic pairing symmetry and strong electronic correlation.

Despite their importance to better understanding of cuprate superconductivity, the infinite-layer n-type cuprates are very difficult to synthesize, and the lack of single-phased compounds with high volume fraction of superconductivity has hindered research progress until a recent breakthrough [116,117]. Using high-pressure (~ 4 GPa) and high-temperature (~ 1000 °C) annealing conditions, Jung *et al.* have been able to achieve single-phased $Sr_{0.9}Ln_{0.1}CuO_2$ compounds with nearly ~ 100% superconducting volume [116]. The availability of these high-quality infinite-layer cuprates has enabled our STS studies of the quasiparticle tunnelling spectra and the pairing symmetry, yielding some curious characteristics that defy widely accepted notions derived from ptype cuprate superconductors [9, 10].

First, the quasiparticle tunnelling spectra and the superconducting energy gap Δ appear to bemomentum-independent, as manifested by spectra taken on more than 300 randomly oriented single crystalline grains [9, 10] and exemplified in Figure 7. Second, the ratio of $(2\Delta/k_BT_c)$ ~ 7 for T_c= 43 K is much larger than the BCS ratio (~ 3.5) for weak coupling *s*-wave superconductors. Third, no discernible satellite features exist in the quasiparticle spectra, in sharp contrast to those of all p-type cuprates, as manifested by the two insets of in Figure 6 for normalized tunnelling spectra taken on optimally doped YBCO and $Sr_{0.9}La_{0.1}CuO_2$ (La-112). It is worth noting that in the context of *t-J* or Hubbard model, the satellite features are strictly associated with *d*-wave pairing symmetry [5, 52,107,108]. Fourth, the tunnelling gap features completely vanish above T_c, suggesting the absence of a pseudogap [9,10], which is also

independently verified by NMR experiments [11]. Fifth, the global response of the system is fundamentally different from that in ptype cuprates, being insensitive to non-magnetic impurities such as Zn up to 3% and extremely susceptible to magnetic impurities such as Ni so that superconductivity becomes completely suppressed with <3% Ni substitution [9,10,117], as manifested in Figure 8

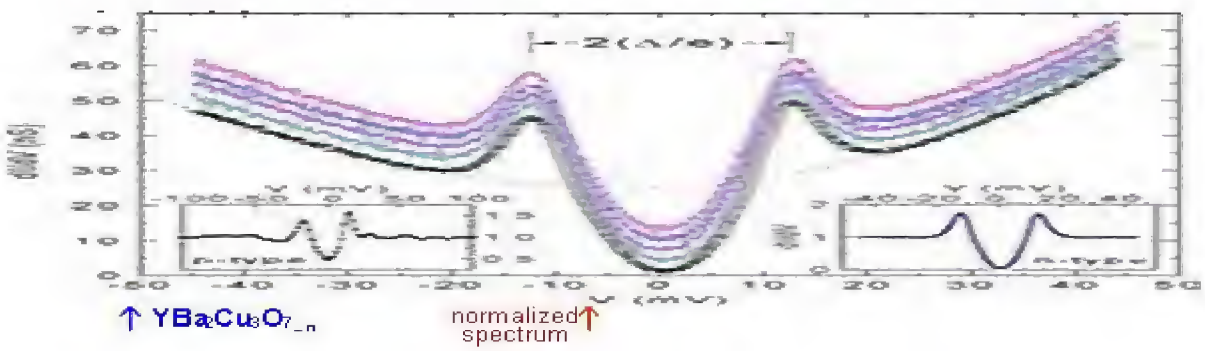

Figure 7: Main Panel Representative Quasiparticle Spectra Taken on Pure $Sr_{0.9}La_{0.1}CuO_2$

As described in the previous subsection, cuprate superconductors with $d_x2_{-y}2$ pairing symmetry are strongly affected by both magnetic and nonmagnetic quantum impurities in the CuO_2 planes. On the other hand, superconductors with *s*-wave pairing symmetry are insensitive to a small concentration of non-magnetic impurities due to the fully gapped Fermi surface and therefore limited interaction with the low-energy excitations at low temperatures [80]. Thus, the global response of the infinite-layer system to quantum impurities is indeed consistent with *s*-wave pairing symmetry. Assuming the validity of the Abrikosov-Gor'kov theory [75], we estimate $J \sim 0.3$ eV [113] for $Sr_{0.9}La_{0.1}CuO_2$ with a critical magnetic impurity concentration $x_c \sim 3\%$. This exchange energy is comparable to but somewhat larger than the Cu^{2+}-Cu^{2+} antiferromagnetic coupling constant.

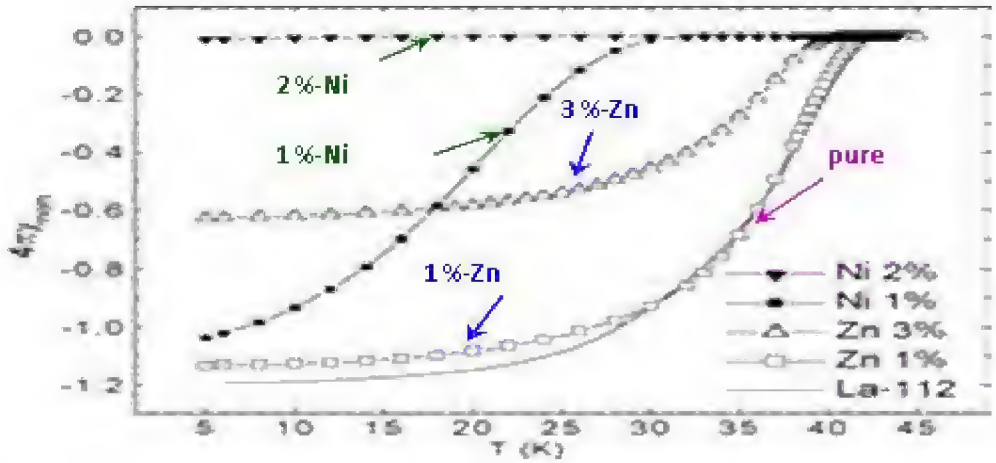

Figure 8: Bulk Magnetic Susceptibility Data of Pure$Sr_{0.9}La_{0.1}CuO_2$ (La-112) and those with Small Concentrations of Impurities. While the Superconducting Volume Consistently Decreases with Increasing Impurities, the Superconducting Transition Temperature ($T_c \sim 43$ K for Pure La-112) Reveals Little Dependence on Spinless Zn-Impurity Substitution up to 3% and Drastic Decrease of with Magnetic Ni-Impurity Substitution [9,117]

Although the momentum-independent pairing potential Δ is supportive of a fully gapped Fermi surface, details of the spectral characteristics appear different from those of weak-coupling isotropic *s*-wave superconductors. To examine whether the discrepancy may be the simple result of anisotropic pair potential, we have performed the generalized BTK analysis [16, 21, 22] and concluded that any anisotropy exceeding 8% should have yielded resolvable momentum

dependentvariations in the quasiparticle spectra [113], as exemplified in Figure 8. So what may have been the physical origin for the excess sub gap quasiparticle DOS (see the right inset of Figure 7 in the infinite-layer cuprates despite a momentum-independent energy gap and the vanishing quasiparticle DOS at the zero bias that rules out disorder-induced effects? The answer may lie in the unusual low-energy excitations in ntype cuprates. That is, the deviation from the spectra of conventional *s*-wave superconductors may be attributed to the coupling of thermally induced quasiparticles to the background SDW. As stated before, the low-energy spin excitations in n-type superconducting cuprates are gapless SDW according to neutron scattering experiments [117]. These low-energy excitations are absent in conventional s-wave superconductor

yielding generally lower T $_c$ in n-type cuprates.

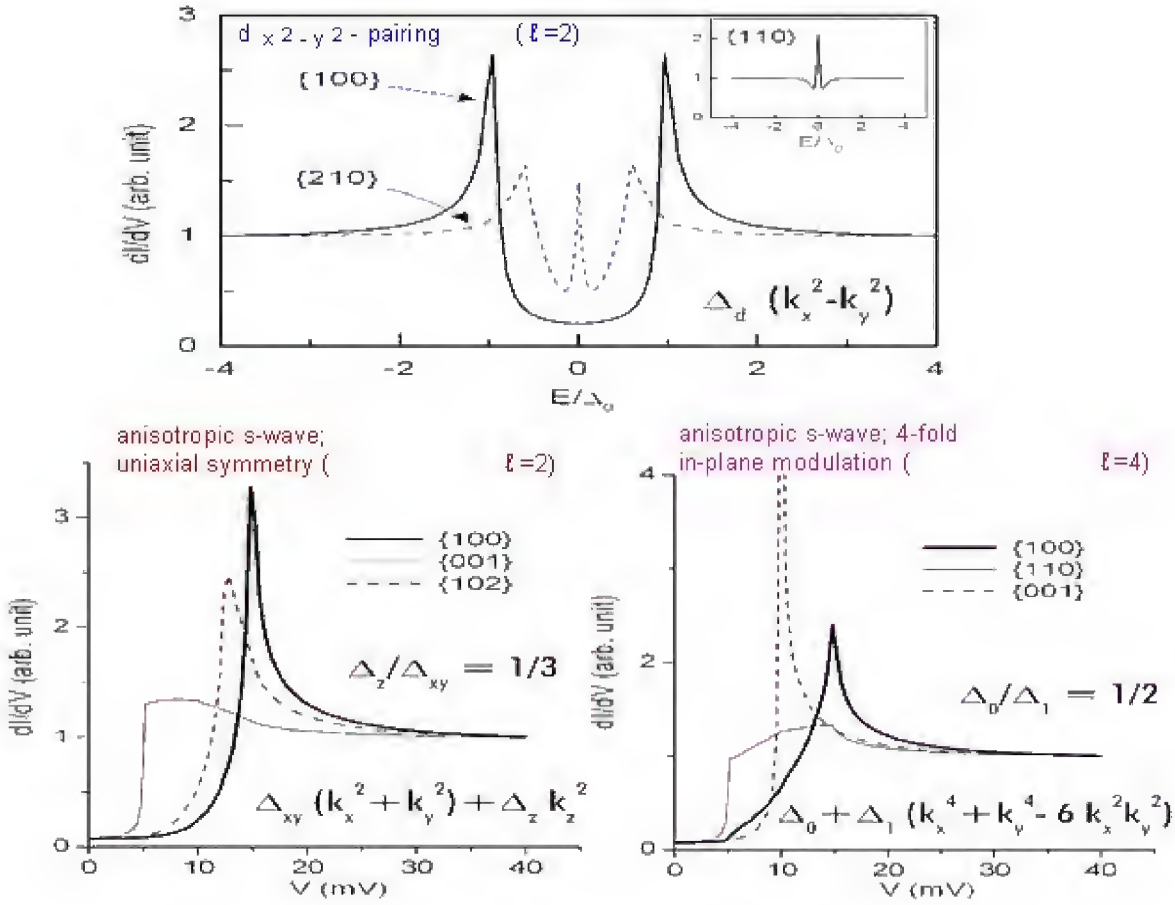

Figure 9: Calculated Quasipartical Tunnelling Spectra for Various Pairing Symmetries with Anisotropic Pairing Potentials Δ_k as given. Upper Panel Corresponds to Different Quasiparticle Tunnelling Momenta into a Pure d-Wave Superconductor. The Lower Left Panel Corresponds to Those of an Anisotropic Swave Pairing Potential with Uniaxial Symmetry and the Lower Right Panel Depicts the Spectra of Anisotropic S-Pairing with 4 Fold in-Plane Modulations [113]

Besides the momentum-independent spectral characteristics and excess sub-gap quasiparticle DOS associated with the infinite-layer cuprates, the absence of discernible satellite features is also noteworthy, as manifested in the inset of Figure 10. We have described in previous sections that the satellite features in p-type cuprates can be attributed to quasiparticle damping by gapped spin excitations along the Cu-O bonding direction [107,108]. Hence, the absence of such satellite features is consistent with the absence of gapped incommensurate spin fluctuations and *s*-wave superconductivity in the infinite-layer system.

Further verification for the pairing symmetry can be made via studying the response of the superconductor to magnetic and non-magnetic impurities. As shown in Figure 8 the bulk response of the infinite-layer system to quantum impurities differs substantially from that of p-type cuprates [117] and resembles that of conventional *s*-wave superconductors. Moreover, detailed investigation of the local quasiparticle spectra reveals additional support for the s-wave pairing symmetry in the infinite-layer system. That is, the tunnelling gap value of optimally doped La-112 with 1% Zn impurities remains comparable to that of pure La112 with no apparent spatial variations, although excess sub-gap quasiparticle density of states exists due to disorder [9,10,113]. In contrast, significant particle-hole asymmetry is induced in the quasiparticle tunnelling spectra of the La-112 sample with 1% Ni impurities [9, 10,113], as shown in Figure 10 (a). The long range impurity induced density of states in Figure 10 (b) is also consistent with the extended Shiba states [76] for magnetic impurity bands in *s*-wave superconductors, and only one bound-state energy $|\Omega_B| \sim 5$ meV can be identified [113], in contrast to the local quasiparticle spectra near magnetic impurities in *d*-wave superconductors [95,102] where strong quasiparticle spectral variations near a magnetic impurity and two different impurity induced resonant energies are observed. It is interesting to note that the exchange interaction J derived from Eq. (3) with empirical values of $|\Omega_B|$, Δ_0 and $N_F$is also consistent with the estimate using Abrikosov-Gorkov theory [75] with a critical magnetic concentration $x \sim 0.3$ [113]. Hence, all spectral characteristics of the Substituted La-112 sample are consistent with those of a strongly correlated *s*-wave pairing superconductor.

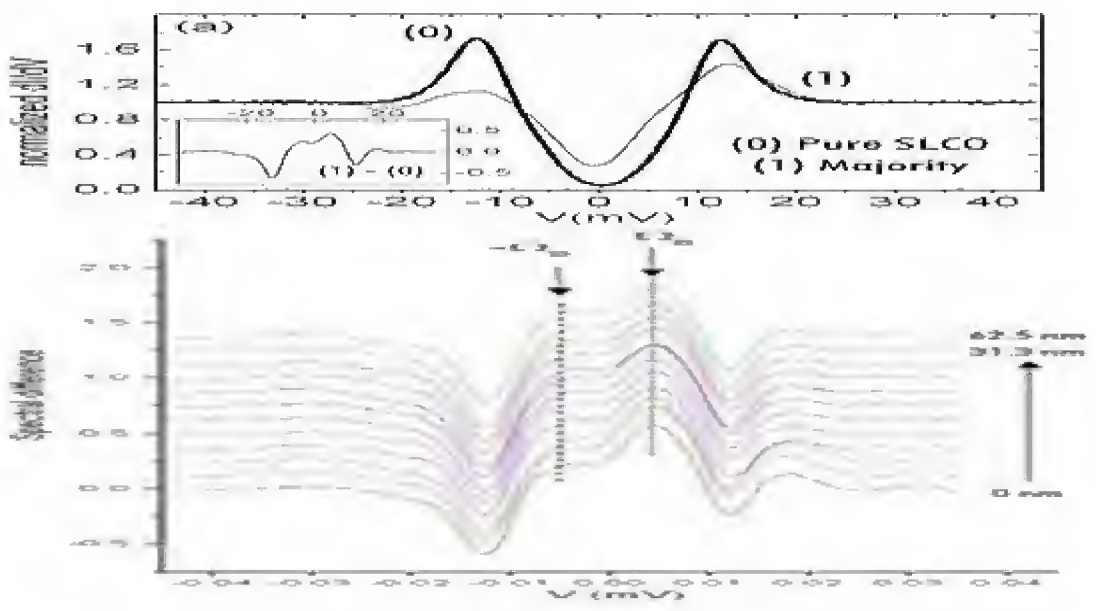

Figure 10: (a) Comparison of the Quasiparticle Spectra Taken on Pure $Sr_{0.9}La_{0.1}CuO_2$ and on $Sr_{0.9}La_{0.1}(Cu_{0.99}Ni_{0.01})O_2$ at 4.2 K. The Inset Illustrates the Spectral Taken on Pure $Sr_{0.9}La_{0.1}CuO_2$ and on $Sr_{0.9}La_{0.1}(Cu_{0.99}Ni_{0.01})O_2$ at 4.2 K. The Inset Illustrates the Spectral Difference of the Two Spectra in the Main Panel, Which Corresponds to Ni-Impurity Contributions (b) Long-Range Spatial Extension of the Impurity Spectral Contribution. The Spectra Have Been Shifted Vertically in the Graph for Clarity. These Spectra Appear to be Quite Homogeneous over Long Range within Each Grain, Consistent with the Shiba States for Impurity Bands. Two Asymmetric Bound-State Energies in the Electron-Like and Hole-Like Branches are Visible at $|\Omega_B| \sim 5$ meV, Corresponding to J ~ 0.3 eV for $\Delta_0 = 13$ meV. (See Ref. [113] for More Details

In addition to *s*-wave pairing symmetry, the optimally doped La-112 system exhibits complete absence of pseudogap above T_c from both tunnelling studies [9, 10] (Figure 11) and the Knight Shift measurements [11]. Recent tunnelling spectroscopic studies of the one-layer n-type cuprates $Pr_{2-x}Ce_xCuO_{4-y}$ [12] also reveal no pseudogap phenomenon above T_c for a wide range of doping levels in zero field, while the application of high magnetic fields

at $T << T_c$ results in an effective pseudogap at $T^* < T_c$ for several underdoped samples, with T^* decreasing with increasing electron doping and vanishing at the optimal doping level. Hence, the pseudogap phenomenon is obviously not a precursor for superconductivity in n-type cuprates.

2.3. Remark on the Origin of the Pseudogap

Regarding the physical origin of the pseudogap phenomenon, we conjecture that in p-type cuprates the decreasing zero-field T^* with increasing hole doping may be correlated with gapped spin excitations such as the incommensurate spin fluctuations [24-28] or triplet pair excitations [5,52], so that the decreasing spin stiffness with increasing doping naturally yields a decreasing T^*. The gapped spin excitations implyspin-singlet states exist between T_c and T^*, which are effectively preformed pairs with physical properties different from those of conventional Fermi liquid. In contrast, the presence of gapless SDW excitations in n-type cuprates may imply that spin-singlet pairs cannot exist above T_c because of the incompatibility of SDW with spinless singlet pairs once the superconducting gap vanishes. On the other hand, the application of a large magnetic field competes with the background AFM spin correlation, so that the resulting low-energy spin excitations in n-type cuprates could change from gapless SDW to gapped spin-flip processes, thereby yielding an effective pseudogap. Moreover, the energy cost for spin flips under a constant magnetic field is expected to decrease with decreasing spin stiffness, which is consistent with a decreasing field-induced T^* that decreases with the increasing doping level. Thus, our conjecture of the pseudogap being a manifestation of quasiparticle damping by gapped spin excitations in doped cuprates has provided a consistent phenomenology for the following experimental facts: 1) the doping dependence of T^* in p-type cuprates; 2) the nonFermi liquid behaviour in the pseudogap regime of p-type cuprates.; 3) the absence of zero-field pseudogap and the doping dependence of a field induced pseudogap in n-type cuprates; and 4) the excess sub-gap quasiparticle DOS in n-type cuprates at $T << T_c$.

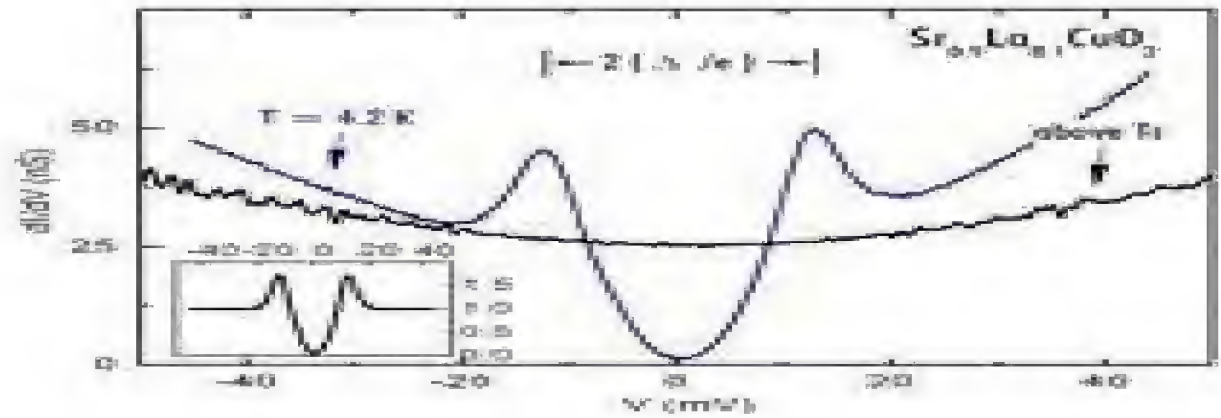

Figure 11: Comparison of the Tunnelling Spectra of $Sr_{0.9}La_{0.1}CuO_2$ Taken at T = 4.2 K (~ 0.1 T_c) and at T >~ T_c, Showing Complete Absence of Any Pseudogap Above T_c

2.4. Competing Orders in the P-Type Cuprate Superconductors

In the presence of competing orders, a specific order parameter can prevail if other orders are suppressed by external variables. For instance, doping dependence of the resistive state properties of various p-type cuprates has been investigated by applying large magnetic fields at low temperatures, with a metal-to-insulator crossover behaviour found at a doping level well below the optimal doping [113], implying no QCP near the optimal doping. On the other hand, neutron scattering studies of the vortex state of $La_2xSr_xCuO_4$ (x = 0.16 [110] and 0.12 [111]) and $La_{1.875}Ba_{0.125-x}Sr_xCuO_4$ [102] have revealed that the AFM spin ordering within the vortex core is enhanced to the extent comparable to that in the normal state,

while the spin correlation extends over a spatial range substantially longer than the vortex-vortex separation [112]. Moreover, the spin correlation exhibits $8a_0$-periodicity, suggesting a related $4a_0$-periodicity for the charge [100]. This interesting observation associated with the vortex cores of p-type cuprates is further corroborated by the STS studies of an optimally doped Bi-2212 system, where directly observation of $4a_0$ $4a_0$ checker-board low-energy (< 12 meV) charge structures within the vortex cores are made [103]. The spectroscopic findings were initially interpreted as the manifestation of competing AFM and superconductivity [58, 60]. That is, the AFM spin order and the accompanying charge order is presumably enhanced due to the suppression of superconductivity in the vortex core and in the regions surrounding the vortex cores due to the presence of induced super currents [58, 60]. However, further STS studies of the Bi2212 system in the absence of field [104] also reveal similar checker-board patterns for large areas of the sample, prompting revaluation of the original interpretation [104]. By performing Fourier analyses on the energy-dependent spatial conductance modulations of the spectra, dispersion relations consistent with those derived from angular resolved photoemission spectroscopy (ARPES) [115,106] are found. This finding suggests that the zero-field conductance modulations in STS data of Bi-2212 are primarily the result of interferences due to elastic scattering of quasiparticles between states of equivalent momenta on the Fermi surface of the superconductor [104]. This simple explanation has effectively ruled out the possibility of charge stripes as a competing order in the Bi-2212 system, because the presence of charge stripes would have resulted in momentum-independent Fourier spectra, in contrast to the strongly dispersive spectra [104]. As for the excess checker-board like conductance modulations within the vortex cores under the application of large dc magnetic fields [103], it is yet to be verified whether a similar scenario, based on quasiparticle interferences due to elastic scattering between equivalent states on the field-driven normal-state Fermi surface, can account for the large magnitude of conductance modulations inside the vortex core [103,104]. It is worth noting that the quasiparticle interference scenario [114] cannot easily account for either the magnetic field induced enhancement of AFM spin correlations [100-112] or the metal-to-insulator transition [109] in the La-Sr (Ba)-Cu-O system. Hence, competing orders of AFM and superconductivity may still be relevant when one considers the field-induced effects on cuprate superconductivity.

Another seemingly controversial issue regarding the spatial variation of the superconducting order parameter in different cuprates [15,105,106] can also be understood in the context of competing orders. That is, it has been noted recently from STS studies that Nano-scale variations exist in the tunnelling gap of the Bi-2212 system [105,106], with Nano-scale regions of sharp superconducting coherence peaks embedded in a less superconducting background of pseudogap-like broadened tunnelling peaks in the spectra. These Nano-scale regions are comparable in size while the density of these regions increases linearly with hole-doping level [105], and the spectra eventually become spatially homogeneous for strongly overdoped samples [107]. On the other hand, no such Nano-scale variations can be found in the YBCO system, as manifested by STS studies of a wide doping range of YBCO samples that revealed the long-range (~ 100 nm) spatially homogeneous spectral characteristics [9,15], and by NMR studies of similar systems [108]. The different behaviour between YBCO and Bi-2212 can be understood as two types of doped Mott insulators that respond differently to the doping level, similar to the different response of type-I and type-II superconductors to an applied magnetic field [109]. More specifically, consider two competing phases A and B in a strongly correlated electronic system, as schematically illustrated in Figure 11. Depending on the magnitude of the effective inertia and interaction potential in the Hamiltonian of the physical system, different behaviour as a function of the chemical potential (μ) can exist [5,110,111]. If Phases A and B are separated by a first-order critical point or a critical line as depicted in Figure 12(a),

Nano-scale phase separations can occur for $\mu \sim \mu_c$. On the other hand, if Phases A and B can coexist over a range of doping levels, as depicted in Figure 12(b), the sample would reveal long range phase homogeneity for the intermediate doping range. Finally, glassy behaviour would occur in the crossover regime if disorder dominates between Phases A and B, as shown in Figure 12(c). Thus, the Nano-scale order-parameter variations in Bi-2212 may be associated with the phase diagram in Figure 12(a) while the long-range spatially homogeneous order parameter in YBCO may be related to the phase diagram in Figure 12(b).

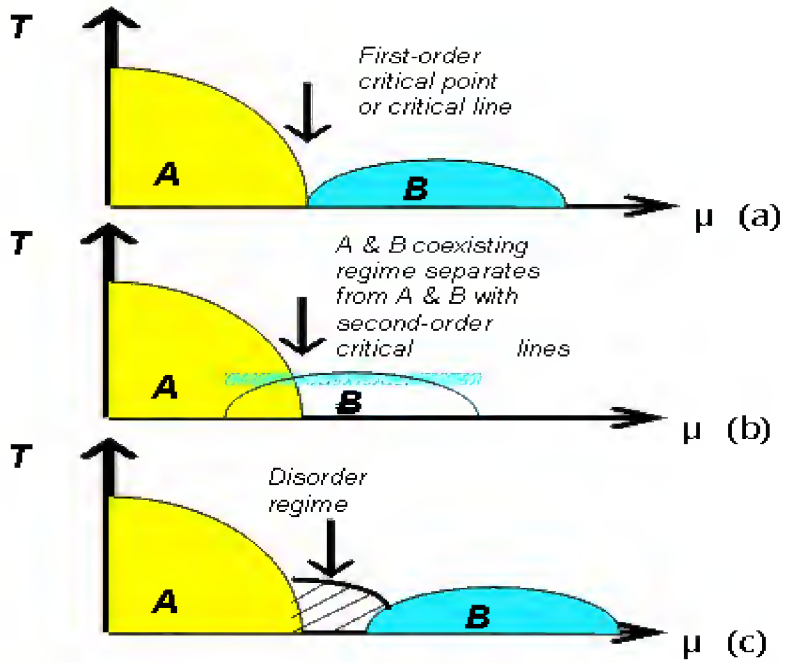

Figure 12: Possible Temperature (T) vs. Chemical Potential Phase (μ) Diagrams for Two Competing Phases A and B Different Behaviour Depends on the Energy Scales of Competing Terms in the Hamiltonian

The question is: what may be the relevant competing phases in YBCO and Bi-2212, and what may be the differences between YBCO and Bi-2212 that give rise to varying spatial homogeneity in the superconducting order parameter? We speculate that the competing orders in the p-type cuprates may be the pseudogap phase and the superconducting state. The former corresponds to a phase with incommensurate gapped spin excitations and the latter is an effective spin liquid. On the difference(s) between YBCO and Bi-2212 that may be responsible for determining the magnitude and sign of the domain wall energy between the competing phases, we suspect that the large anisotropy inBi-2212 (particularly in underdoped samples) versus the stronger three dimensional coupling in YBCO may contribute to the occurrence of Nano-scale phase separations in the former.

This issue awaits further theoretical investigation. We also remark that the formation of Nano-scale phase separations is by no means a necessary condition for superconductors with short coherence lengths, as some might have naively assumed. In fact, different ground states as a function of the chemical potential have also been observed in the perovskite manganite's $Ln_1xM_xMnO_3$ (Ln: La, Nd, Pr, M: Ca, Sr, Ba), which are strongly correlated electronic systems showing colossal negative magneto resistance (CMR) effects [110-112]. Depending on the doping level and the chemical composition, the competing phases of ferromagnetism (FM) and AFM in the manganite's can result in Nano-scale inhomogeneity in the magnetic order parameter, as empirically manifested by STM imaging [112] and theoretically verified via numerical calculations [110,111]

4. FURTHER DISCUSSIONS & OUTLOOK

After reviewing a wide variety of experimental information associated with both p-type and n-type cuprates, it is clear that no obvious particle-hole symmetry exists in these doped Mott insulators, so that the simple approach of a one-band Hubbard model cannot provide a universal account for all experimental findings. In particular, it appears that only two commonalities can be identified among all families of cuprates. One is the strong electronic correlation and the other is the AFM spin correlation in the CuO_2 planes [9, 10]. A number of important phenomena previously deemed as essential to cuprate superconductivity are in fact not universal, including the $d_{x^2-y^2}$ pairing symmetry, the pseudogap phenomena and incommensurate spin fluctuations. These latest experimental developments have thus imposed stringent constraints on existing theories.

Can a sensible physical picture emerge from all experimental facts associated with both p-type and n-type cuprates while simultaneously reconcile a number of seemingly conflicting observations? Empirically, we note that an important difference between p-type and n-type cuprates is in the low energy spin excitations, although both systems retain short-range AFM Cu^{2+}-Cu^{2+} spin correlation in their superconducting state [6, 25-28,117]. For arbitrary doping levels, incommensurate spin fluctuations could occur along the Cu-O bonding direction of p-type cuprate superconductors. These spin fluctuations are gapped and are therefore suppressed in the ground state. The anisotropic spin excitation gap, quasi-two dimensionality and the tendency to minimize on-site Coulomb repulsion in p-type cuprates could conspire to yield the lowest ground state energy under pair wave functions with $d_{x^2-y^2}$-symmetry. Moreover, for a given doping level, the incommensurate spin excitation gap of p-type cuprates is always larger than or comparable to the superconducting gap [25-28], implying that singlet pairing of carriers can exist in the CuO_2 planes at temperatures below the incommensurate spin excitation gap, and that the relevant mean-field energy scale is Ω_{res} rather than the AFM exchange energy J. This scenario is consistent with the presence of a pseudogap and the existence of singlet pairs in the pseudogap regime ($T_c < T < T^*$) of the p-type cuprates. Moreover, the fluctuation effects in the pseudogap regime are primarily associated with the charge rather than the spin degrees of freedom.

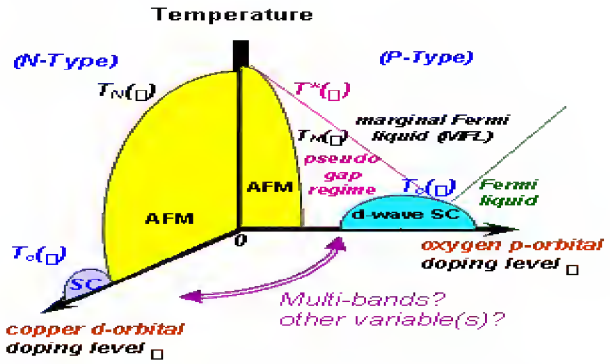

Figure 13: An Attempt to Unify the Phase Diagrams of p-Type and n-Type Cuprates May Requirethe Consideration of Additional Degrees of Freedom

On the other hand, the low-energy spin excitations in n-type cuprates are gapless SDW [117]. The presence of SDW in the superconducting state could hinder singlet pairing because of the tendency of misaligned spin orientation for pairs over a finite spatial distance, thus yielding generally lower T_c values in one-layer n-type cuprate superconductors relative to one-layer ptype cuprates. The absence of gapped incommensurate spin excitations in n-type cuprates is also consistent with the absence of pseudogap. As for the pairing symmetry, it is conceivable that the combined effects of

strong three dimensional electronic coupling in the infinite-layer system (see Figure 3), the existence of isotropic SDW excitations and the degeneracy of $d_x2_{-y}2$ and $d_{3z}2_{-r}2$-orbitals would favour*s*-wave pairing symmetry in the ground state. On the other hand, the quasi-two dimensionality energy in the one-layer n-type cuprates may compete with the aforementioned energy scales so that the overall energy difference between *s*- and $d_x2_{-y}2$-wave pairing is small and strongly dependent on the doping level and oxygen disorder.

Despite the consistency of the above scenario with most experimental observation, it provides no microscopic description for the Cooper pairing in the CuO_2 planes. While it is clear that AFM spin correlation plays an important role in the pair formation and pseudogap phenomena, the link to unifying the phase diagrams of p-type and n-type cuprates is yet to be identified. Meanwhile, most phenomenology such as the stripe scenario or the DDW model can be regarded as special cases of competing orders rather than a sufficient condition for cuprate superconductivity. Thus, the primary theoretical challenge is to address the inadequacy of one-band Hubbard model and to examine whether multi-band approximation or inclusion of other variable(s) may be necessary in the quest of unifying the phenomenology of all cuprates, as schematically illustrated in Figure 13. Ultimately, the development of an adequate microscopic theory for this strongly correlated electronic system must prescribe an effective attractive pairing interaction among carriers that suffer strong on-site Coulomb repulsion. The effective attraction may result from unique pair wave functions with optimized orbital and spin degrees of freedom that minimize the Coulomb repulsion, and the resulting effective attraction is likely to be only moderate compared with the bare Coulomb energy. In fact, the possibility of a moderate-to-small effective attraction may explain why certain physical properties associated with the cuprates can be reasonably modelled with the BCS approximation, although it is highly probable that the pairing mechanism for cuprate superconductivity is fundamentally different from conventional electron-phonon mediated BCS superconductivity, and may unavoidably involve magnetism.

5. CONCLUDING REMARKS

The discovery and subsequent intense research of high-temperature superconducting cuprates have revolutionized our understanding of superconductivity and strongly correlated electronic materials. We have reviewed in this article some of the recent experimental developments and the status of various theoretical scenarios, and have suggested that many interesting experimental findings can be understood in terms of competing orders. On the other hand, the apparent differences among hole doped (p-type) and electron-doped (n-type) cuprates are indicative particle-hole asymmetry and of the inadequacy of considering the cuprates in terms of a one-band Hubbard model. It is conjectured that different forms of low-energy spin excitations in the cuprates, i.e. gapped incommensurate spin fluctuations in the p-type and gapless SDW in the n-type, may play an important role in determining the ground state and low-energy excitation spectra of the corresponding cuprate superconductors.

In particular, the pseudogap phenomenon may be associated with the gapped incommensurate spin excitations, and therefore is absence in n-type cuprates. The pairing symmetry is also non-universal and appears to be a consequence of competing orders. The only ubiquitous properties among all cuprates are the strong electronic correlation and AFM spin interaction in the CuO_2 planes. Future research challenge will require the convergence of empirical facts and the development of a microscopic theory that unifies all experimental observation and provides an effective attractive interaction for pair formation in the CuO_2 planes of the cuprates.

6. REFERENCES

1. J. G. Bednorz and K. A. Muller: Z. Phys. **B64**, 189 (1986).
2. J. Orenstein and A. J. Millis, Science **288**, 468 (2000).
3. S. Sachdev: Science **288**, 475 (2000).
4. M. Vojta, Y. Zhang, and S. Sachdev, Phys. Rev. B **62**, 6721 (2000).
5. S.-C. Zhang: Science **275**, 1089 (1997); S.-C. Zhang et al.: Phys. Rev. B **60**, 13070 (1999).
6. M. A. Kastner et al.: Rev. Mod. Phys. **70**, 897 (1998).
7. M. B. Maple, MRS Bulletin, Vol.**15**, No. 6, pp. 60 -- 67 (1990).
8. T. Timusk and B. Statt, Rep. Prog. Phys. **62**, 61 (1999).
9. N.-C. Yeh et al.: Physica C **367**, 174 (2002) [10] C.-T. Chen et al.: Phys. Rev. Lett. **88**, (2002).
10. G. V. M. Williams et al.: Phys. Rev. B **65**, 224520 (2002).
11. L. Alff et al.: private communications (2002).
12. D. J. Van Harlingen: Rev. Mod. Phys. **67**, 515 (1995).
13. C. C. Tsuei and J. R. Kirtley, Rev. Mod. Phys. **72**, 969 (2000).
14. N.-C. Yeh et al.: Phys. Rev. Lett. **87**, 087003 (2001); Physica C **364-365**, 450 (2001).
15. J. Y. T. Wei et al.: Phys. Rev. Lett. **81**, 2542 (1998); Physica B **284**, 973 (2000).
16. L. Alff et al. Phys. Rev. Lett. **83**, 2644 (1999).
17. C. C. Tsuei and J. R. Kirtley: Phys. Rev. Lett. **85**, 182 (2000).
18. J. A. Skinta et al.: Phys. Rev. Lett. **88**, 207005 (2002).
19. A. Biswas et al.: Phys. Rev. Lett. **88**, 207004 (2002)
20. C. R. Hu, Phys. Rev. Lett. **72**, 1526 (1994).
21. Y. Tanaka and S. Kashiwaya, Phys. Rev. Lett.**74**, 3451 (1995).
22. N. P. Armitage et al.: Phys. Rev. Lett. **88**, 257001 (2002).
23. V. J. Emery, S. A. Kivelson and J. M. Tranquada, Proc. Natl. Acad. Sci. USA **96**, 8814 (1999); cond-mat/9907228.
24. N. Ichikawa et al.: Phys. Rev. Lett. **85**, 1738 (2000).
25. M. Fujita et al.: Phys. Rev. Lett. **88**, 167008 (2002).
26. H. A. Mook, P. Dai, and F. Doğan: Phys. Rev. Lett. **88**, 097004 (2002).
27. J. M. Tranquada et al.: Nature **375**, 561 (1995); Phys. Rev. Lett. **78**, 338 (1997).

28. S. Chakravarty et al.: Phys. Rev. B **63**, 094503 (2001); S. Chakravarty and H.-Y. Kee, Phys. Rev. B **61**, 14821 (2000).

29. I. K. Affleck and J. B. Marston; Phys. Rev. B **37**, 3774 (1988).

30. P. W. Anderson et al.: Phys. Rev. Lett. **58**, 2790 (1987); and P. W. Anderson: Science **235**, 1196 (1987).

31. P. W. Anderson and Z. Zou: Phys. Rev. Lett. **60**, 132 (1988); P. W. Anderson and Y. Ren:Ann. N.Y. Acad. Sci. **581**, 44 (1990).

32. G. Kotliar, Phys. Rev. B **37**, 3664 (1988).

33. D. A. Bonn et al.: Nature **414**, 887 (2001).

34. C.-C. Fu, Z. Huang, and N.-C. Yeh: Phys.Rev. B **65**, 224516 (2002).

35. P. W. Anderson: Science **268**, 1154 (1995).

36. A. J. Leggett: Science **274**, 587 (1996).

37. A. A. Tsvetkov et al.: Nature **395**, 360 (1998).

38. D. Pines: Physica C **235**, 113 (1994).

39. D. Scalapino: Phys. Rep. **250**, 329 (1995).

40. P. A. Lee and N. Reed: Phys. Rev. Lett. **58**, 2891 (1987).

41. V. J. Emery and S. A. Kivelson: Nature **374**, 434 (1995).

42. Y. J. Uemura, G. M. Luke, B. J. Sternleib et al.: Phys. Rev. Lett. **62**, 2317 (1989).

43. V. J. Emery, S. A. Kivelson, and O. Zachar, Phys. Rev. B **56**, 6120 (1997).

44. G. Siebold, C. Castellani, D. DiCastro, M. Grilli, Phys. Rev. B **58**, 13506 (1998).

45. V. B. Geshkenbein, L. B. Ioffe and A. I. Larkin: Phys. Rev. B **55**, 3173 (1997).

46. Q. Chen et al.: Phys. Rev. Lett. **81**, 4708 (1999); I. Kosztin et al.: Phys. Rev. B **61**, 11662 (2000).

47. T. Senthil and M. P. A. Fisher, Phys. Rev. Lett. **86**, 292 (2001); Phys. Rev. B **62**, 7850 (2000).

48. C. M. Varma, Phys. Rev. B **55**, 14554 (1997); Phys. Rev. B **61**, R3804 (2000).

49. P. A. Lee and N. Nagaosa: Phys. Rev. B **46**, 5621 (1992).

50. P. A. Lee and X. G. Wen: Phys. Rev. Lett. **78**, 4111 (1997).

51. E. Demler and S.-C. Zhang: Phys. Rev. Lett. **75**, 4126 (1995).

52. A. J. Leggett: J. Phys. (Paris), Colloq. **41**, C7 (1980).

53. F. C. Zhang and T. M. Rice: Phys. Rev. B **37**, 3759 (1988).

54. S. Charkravarty, B. I. Halperin and D. R. Nelson, Phys. Rev. B **39**, 2344 (1989).

55. A. V. Chubukov, S. Sachdev and J. Ye, Phys. Rev. B **49**, 11919 (1994).

56. J. R. Schrieffer, X. G. Wen and S. C. Zhang, Phys. Rev. B **39**, 11663 (1989).

57. S. Sachdev and S. C. Zhang, Science **295**, 452 (2002).

58. D.-H. Lee, Phys. Rev. Lett. **88**, 227003 (2001).

59. E. Demler, S. Sachdev, and Y. Zhang, Phys. Rev. Lett. **87**, 067202 (2001).

60. J. X. Zhu and C. S. Ting, Phys. Rev. Lett. **87**, 147002 (2001).

61. J. H. Han and D.-H. Lee, Phys. Rev. Lett. **85**, 1100 (2000); J. H. Han, Q. H. Wang and D.-H. Lee, Phys. Rev. B **64**, 064512 (2001).

62. J. Kishine, P. A. Lee and X.-G. Wen, Phys. Rev. Lett. **86**, 5365 (2001).

63. D. S. Rokhsar, Phys. Rev. Lett. **70**, 493 (1993).

64. M. Sigrist, D. B. Bailey and R. B. Laughlin, Phys. Rev. Lett. **74**, 3249 (1995); R. B. Laughlin, Phys. Rev. Lett. **80**, 5188 (1998).

65. L. Alff et al.: Phys. Rev. B. **58**, 11197 (1998); Phys. Rev. B. **55**, 14757 (1997).

66. I. Iguchi et al.: Phys. Rev. B **62**, R6131 (2000); W. Wang et al.: Phys. Rev. B **60**, 42721 (1999).

67. J. R. Kirtley, C. C. Tsuei, and K. A. Moler, *Science***285**, 1373 (1999).

68. N.-C. Yeh et al.: Physica C **341-348**, 1639 (2000).

69. M. Fogelstrom, D. Rainer and J. A. Sauls, Phys. Rev. Lett. **79**, 281 (1997).

70. M. Covington et al., Phys. Rev. Lett. **79**, 277 (1997).

71. F. Tafuri and J. R. Kirtley, Phys. Rev. B **62**, 13934 (2000).

72. Y. Asano and Y. Tanaka, Phys. Rev. B **65**,064522 (2002)

73. Y. Tanaka et al., Physica C **367**, 73 (2002).

74. A. A. Abrikosov and L. P. Gor'kov, Soviet Phys. JETP **12**, 1243 (1961).

75. H. Shiba, Prog. Theor. Phys. **40**, 435 (1968).

76. P. Fulde and R. A. Ferrell, Phys. Rev. **135**, A550 (1964).

77. M. A. Wolf and F. Reif, Phys. Rev. **137**, A557 (1965).

78. P. Schlottmann, Phys. Rev. B **13**, 1 (1976).

79. P. W. Anderson, J. Phys. Chem. Solids **11**, 26 (1959); Phys. Rev. Lett. **3**, 325 (1959).

80. G.-q. Zheng et al.: J. Phys. Soc. Japan **62**, 2591 (1989); Physica C **263**, 367 (1996).

81. H. Alloul et al.: Phys. Rev. Lett. **67**, 3140 (1991).

82. T. Miyatake et al.: Phys. Rev. B **44**, 10139 (1991).

83. M. Ishida et al.: Phys. Rev. Lett. **76**, 531 (1996).

84. K. Tomimoto et al.: Phys. Rev. B **60**, (1999).

85. N. L. Wang et al.: Phys. Rev. B **57**, R11081 (1999).

86. H. F. Fong et al.: Phys. Rev. Lett. **82**, 1939 (1999).

87. J. Figueras et al.: Supercond. Sci. Technol. **13**, 1067 (2000).

88. J. Bobroff et al.: Phys. Rev. Lett. **83**, 4381 (1999); Phys. Rev. Lett. **86**, 4116 (2001).

89. Y. Sidis et al.: Phys. Rev. Lett. **84**, 5900 (2000).

90. W. A. MacFarlane et al.: Phys. Rev. Lett. **85**, 1108 (2000).

91. S. H. Pan et al.: Nature **403**, 746 (2000).

92. D. Poilblanc, D. J. Scalapino and W. Hanke: Phys. Rev. B **50**, 13020 (1994).

93. A. V. Balatsky, M. I. Salkola and A. Rosengren: Phys. Rev. B **51**, 15547 (1995).

94. M. I. Salkola, A. V. Balatsky and D. J. Scalapino: Phys. Rev. Lett. **77**, 1841 (1996).

95. M. I. Salkola, A. V. Balatsky and J. R. Schrieffer: Phys. Rev. B **55**, 12648 (1997).

96. M. E. Flatte and J. M. Byers, Phys. Rev. B **56**, 11213 (1997); Phys. Rev. Lett. **80**, 4546 (1998).

97. M. I. Salkola and J. R. Schrieffer: Phys. Rev. B **58**, R5952 (1998).

98. R. Kilian et al.: Phys. Rev. B **59**, 14432 (1999).

99. J. X. Zhu and C. S. Ting: Phys. Rev. B **64**, 060501 (2001); Phys. Rev. B **63**, 020506(2001).

100. M. Vojta and R. Bulla, Phys. Rev. B **65**, 014511 (2001); A. Polkovnikov, S. Sachdev and M. Vojta: Phys. Rev. Lett. **86**, 296 (2001).

101. E. W. Hudson et al.: Nature **411**, 920 (2001).

102. A. Yazdani et al.: Science **275**, 1767 (1997).

103. V. Madhavan et al.: Science **280**, 576 (1998).

104. K. M. Lang et al. Nature **415**, 412 (2002).

105. S. H. Pan et al., Nature **413**, 282 (2001).

106. A. V. Chubukov and N. Gemelke, Phys. Rev. B **61**, R6467 (2000); Ar. Abanov and A. V. Chubukov, Phys. Rev. Lett. **83**, 1652(1999).

107. C. L. Wu, C. Y. Mou and D. Chang, Phys. Rev. B **63**, 172503 (2001).

108. A. Lanzara et al., Nature **412**, 510 (2001).

109. V. M. Krasnov et al.; Phys. Rev. Lett. **84**, 5860 (2000).

110. N. Miyakawa et al.: Phys. Rev. Lett. **83**, 1018 (1999); Phys. Rev. Lett. **80**, 157 (1998).

111. Ch. Renner et al.: Phys. Rev. Lett. **80**, 149 (1998).

112. N.-C. Yeh et al.: J. Low Temp. Phys. (2002), (in press); cond-mat/0207594.

113. T. Siegrist et al.: Nature **334**, 231 (1998).

114. M. G. Smith et al.: Nature **351**, 549 (1988).

115. C.U. Jung et al.: Physica C **366**, 299 (2002); M.-S. Kim, cond-mat/0102420.

116. C.U. Jung et al.: Phys. Rev. B **65**, 172501 (2002).

117. K. Yamada et al.: J. Phys. Chem. Solids **60**, 1025 (1999); T. Takahashi et al.: J. Phys. Chem. Solids **62**, 1025 (2001).